Dalton Transactions

ROYAL SOCIETY OF CHEMISTRY

PAPER

View Article Online
View Journal | View Issue

Cite this: *Dalton Trans.*, 2024, **53**, 18998

Unveiling the impact of enhanced hydrophobicity of ZIF-71 on butanol purification: insights from experimental and molecular simulations†

Norma Tiempos-Flores,[a] Oscar I. Arillo-Flores,[b] Eugenio Hernández-Fernández,[a] Victor M. Ovando-Medina,[c] Marco A. Garza-Navarro,[d] Sandra Pioquito-García[a] and Nancy E. Davila-Guzman *[a]

Received 1st September 2024,
Accepted 1st October 2024

DOI: 10.1039/d4dt02485k

rsc.li/dalton

Biofuels offer significant potential for reducing carbon emissions and enhancing energy sustainability, but their efficient purification remains a significant challenge. In this study, the performance of a hydrophobic zeolitic imidazolate framework, ZIF-71(ClBr)-SE, in the adsorptive separation of butanol from single- and ternary-component systems (acetone, butanol, and ethanol) was investigated and compared with ZIF-8 and ZIF-71. Physicochemical characterization techniques, including XRD, SEM, BET, TGA, and DVS, confirmed that the modified ZIF-71 is hydrophobic, isostructural with ZIF-71, and has a higher surface area. Adsorption tests in aqueous solutions revealed that ZIF-71(ClBr)-SE unexpectedly showed a higher affinity for acetone over butanol. DFT molecular simulations provided insights into solute-ZIF interactions, highlighting preferential sites for ZIF interaction.

Introduction

Today fossil fuels remain the main source of energy worldwide. In Mexico, fossil fuels account for 83% of primary energy production (hydrocarbons and coal), while renewable energy represents 15%.[1] Reducing the use of fossil fuels in our daily activities is crucial to counteracting their negative effects on human health and protecting the environment. Energy generation from fossil fuels emits carbon dioxide (CO_2), nitrogen oxide (NO), methane (CH_4), and other gases into the atmosphere, which pollute the air and increase the Earth's average temperature.[2] In this context, promoting alternative energy sources is essential to improving air quality and curbing climate change. These alternative energies, which are clean, long-lasting, and distinct from fossil fuels due to their diversity and abundance, include wind, solar, hydroelectric, and biofuels. The transportation sector is particularly dependent on fossil fuels, contributing 15% of global atmospheric emissions, primarily from road vehicles.[3] Biofuels present an ideal alternative energy source for the transportation sector. Examples of biofuels include biodiesel, bioalcohols (biomethanol, bioethanol, biobutanol), and biogas. Historically, bioethanol has been the most widely used liquid transportation fuel.[4] However, biobutanol is less corrosive, less volatile (it evaporates six times more slowly than bioethanol), can be mixed with gasoline in any proportion, and can even be used at 100% by volume in a conventional internal combustion engine without requiring modifications.[5,6] The increasing production of biobutanol holds promise for reducing fossil fuel consumption in the transportation sector, thereby lowering emissions of polluting gases into the atmosphere.

Biobutanol is produced through the fermentation of sugars by microorganisms, but one of the key challenges in its production is the purification of the aqueous medium in which it is generated. The microorganisms used in this process generally tolerate only low concentrations of butanol, which can inhibit their growth. Depending on the species, this tolerance varies: *Clostridium strains* typically withstand butanol concentrations below 2% v/v, *Lactiplantibacillus plantarum* exhibits tolerance in the 3–4% v/v range, and *Pseudomonas putida* can tolerate up to 6% v/v.[7] Several methods are used for biobutanol purification, including distillation, gas stripping, liquid–liquid extraction, pervaporation, and adsorption.[8] Although distillation is the conventional, and most commonly used method for biobutanol recovery, it is neither economically nor energetically viable. Adsorption has emerged as a promising alterna-

[a]*Universidad Autónoma de Nuevo León, UANL, Facultad de Ciencias Químicas, Av. Universidad, Cd. Universitaria, 66455 San Nicolas de los Garza, Nuevo León, Mexico. E-mail: nancy.davilagz@uanl.edu.mx, nancy.davilagz@gmail.com*
[b]*Universidad Autónoma de Querétaro, UAQ, Facultad de Ciencias Químicas, Mexico*
[c]*Unidad Académica Multidisciplinaria Región Altiplano, Universidad Autónoma de San Luis Potosí, Matehuala, San Luis Potosí, 78700, Mexico*
[d]*Universidad Autónoma de Nuevo León, UANL, Centro de Innovación y Desarrollo de Ingeniería y Tecnología, Apocada, 66600 Nuevo León, Mexico*

† Electronic supplementary information (ESI) available. See DOI: https://doi.org/10.1039/d4dt02485k

tive for the selective separation of biobutanol.[6,9] In this process, biobutanol is adsorbed onto the surface of an adsorbent and then desorbed by increasing the temperature. The adsorbents used in biobutanol enrichment must have high adsorption capacities, greater affinities for alcohol than for water, and large specific surface areas. Various adsorbents, such as activated carbon, polymeric resins, and zeolites, have been employed in the biobutanol separation process.[10] Metal–organic frameworks (MOFs), which consist of inorganic units and organic linkers, offer an advantage over other adsorbents due to their tunability for specific applications.[11] Zeolitic imidazolate frameworks (ZIFs), a subgroup of MOFs, are composed of Zn(II) atoms bonded to nitrogen atoms derived from imidazole molecules, forming structures like zeolites. Depending on the functional groups present in the imidazole ring, ZIFs can exhibit hydrophobic or hydrophilic properties,[12,13] which is a crucial characteristic for the selectivity of the target compound.

ZIFs can exhibit hydrophobicity inside the pores and/or on the external crystal surface. For example, ZIF-8 has hydrophobic internal pore surfaces due to its flexible methyl groups, but its external crystal surface is hydrophilic. In contrast, MAF-6 shows hydrophobicity on both its internal pore surfaces and external surfaces. To investigate these hydrophobic behaviors, water adsorption isotherms at room temperature are typically used to assess the internal pore hydrophobicity, while water contact angle measurements evaluate the external surface hydrophobicity.[14]

Hydrophobic MOFs have been investigated for the removal of alcohols from aqueous solutions due to their ability to inhibit the diffusion of water molecules into the pores of the adsorbent materials, which can enhance separation. For instance, L. Gan *et al.*, studied a hydrophobic MOF composed of copper ions and carborane-carboxylate ligands, known as mCB-MOF-1, which demonstrated excellent stability in both acidic and basic aqueous media. This material exhibited a strong affinity for individual compounds of acetone, butanol, and ethanol. Notably, mCB-MOF-1, carborane-based MOF, achieved higher butanol recovery than ZIF-8 in a real ABE mixture, as confirmed by Monte Carlo and DFT calculations. Furthermore, it displayed a butanol selectivity over ethanol greater than 12.0 at pressures below 25 kPa and 7.0 at 100 kPa, as predicted by the Theory of the Ideal Adsorbed Solution.[15] J. Wang *et al.*, evaluated butanol adsorption using three isostructural hydrophobic ZIFs: ZIF-11, ZIF-71, and MAF-6. Due to the hydrophobic nature of these materials, the results indicated high selectivity for butanol over ethanol and acetone in a synthetic ABE blend. The highest adsorption capacity was observed in MAF-6 with 247.7 mg g^{-1}, compared to ZIF-11 and ZIF-71 which showed capacities of 141.9 and 198.5 mg g^{-1}, respectively. This outcome was attributed to the difference in pore sizes, with MAF-6 having the largest pore opening of 7.4 Å, followed by ZIF-7 (5.1 Å) and ZIF-11 (3.1 Å).[16] J. Song *et al.*, developed ZIF-302-derived adsorbents with varying cage sizes for the separation of acetone/butanol mixtures. The cage size modulation was achieved by adjusting the ratios of 2-methylimidazole (mIm) and 5-methylbenzimidazole (mbIm) ligands. As a result, it was found that ZIF-302 with larger cage size (9.6 Å × 6.6 Å) adsorbed a higher proportion of butanol, while ZIF-302 without smaller cage size (6.5 Å × 6.6 Å) preferentially adsorbed acetone.[17]

Functionalizing organic linkers during MOF construction and post-synthesis modification of these linkers with alkyl chains are among the strategies developed to enhance the hydrophobicity of MOFs.[18] S. Liu *et al.*, worked with a post-synthesis acid-exchange method to obtain a hydrophobic MOF. This method involved dissolving pentadecafluorooctanoic acid (PFOA) in *N*,*N*′-dimethylformamide (DMF), then adding MOF-808 in varying amounts and subjecting the mixture to a reaction at 70 °C for 12 hours. Finally, the sample was washed with DMF and ethanol and dried at 100 °C. This process resulted in the synthesis of the hydrophobic MOF named MOF-808-PFOA. The post-synthesis method improved the hydrophobicity of MOF-808-PFOA, as the contact angle (CA) increased from 19.5° to 134° with the optimal amount of acid.[19] X. Quan *et al.*, hydrophobically modified Fe^{3+}@Cu-MOFs by incorporating Iron(III) meso-tetra(4-carboxyphenyl) porphine chloride (Fe-TCPP) into the Cu-MOF and different long-chain alkyl quaternary ammonium bromides on the surface. The results showed that the longer the chain of the alkyl quaternary ammonium bromides, the higher the contact angle, leading to increased hydrophobicity of the MOFs.[20] Y. Zhou *et al.*, converted the hydrophilic UiO-66-SH MOF into a hydrophobic MOF called UiO-66-RA by introducing rosin acid with double-bond functional groups into the organic linkers. In wetting tests, the UiO-66-SH MOF absorbed water droplets quickly, whereas, with the UiO-66-RA MOF, the water droplets remained round, corresponding to a contact angle of 157 ± 0.5°.[21] In our research, the effect of the enhanced hydrophobicity of ZIF-71 was evaluated in the removal of butanol from the aqueous mixture of acetone, butanol, and ethanol. DTF calculations were used to gain deeper understanding of the interactions in the adsorption process.[22]

Experimental

Chemicals

The reagents used in the experiments were Basolite Z1200 (ZIF-8), zinc acetate dihydrate ($Zn(CH_3COO)\cdot 6H_2O$, 98%) methanol (CH_3OH, 99.8%), sodium formate ($NaCHO_2$), dichloromethane (CH_2Cl_2, 99.9%), distilled water, acetone (CH_3COCH_3, 98%), butanol ($CH_3(CH_2)_3OH$, 99.8%), and ethanol (CH_3CH_2OH, 98%). All chemicals and reagents were purchased from CTR scientific (Monterrey, Mexico) and were used without any additional purification.

Synthesis of ZIF-71(ClBr)-SE

ZIF-71(ClBr)-SE was synthesized according to the procedure that we previously reported.[23] Typically, zinc acetate was dissolved in methanol and then the solution added to another solution consisting of bromo-5-chloroimidazole and sodium

formate fully dissolved in methanol without stirring at room temperature for 24 h. The precipitate was separated by centrifugation (3500 rpm, 5 min), followed by washing methanol three times. Methanol was removed and replaced with dichloromethane by soaking and rinsing the MOF with the new solvent daily over a period of 6 days. Finally, the obtained product was dried under a vacuum for 6 h at 60 °C before being characterized.

Synthesis of ZIF-71

ZIF-71 was synthesized following a previously reported method by Chance *et al.*[24] Separately dissolved in methanol were zinc acetate and 4,5-dichloroimidazole. The zinc acetate solution was then added to the 4,5-dichloroimidazole solution without stirring at room temperature for 24 h. The precipitated obtained was washed with methanol thrice and separated by centrifugation (3500 rpm, 5 min). The final product was dried under a vacuum for 6 h at 60 °C.

Characterization

Powder X-ray diffraction (PXRD) pattern was recorded using a Rigaku ULTIMA IV diffractometer with Cu-Kα (λ = 1.541830 Å) radiation. The range scanned was from 3–50° (2θ) in 0.02° steps and a scan speed of 10° min^{-1}. Sample of ZIF-71(ClBr)-SE was studied by thermogravimetric analysis (TA Instruments, TA550, UK) under N_2 atmosphere at 40 mL min^{-1} and a heating rate of 20 °C min^{-1} from 25 °C to 800 °C. The morphology of the synthesized ZIF-71(ClBr)-SE particles was characterized using a FEI Titan G2 80-300 field emission gun transmission electron microscope (TEM), employing the high-angle annular dark field (HAADF-STEM) imaging technique. Nitrogen sorption isotherms at 77 K were determined using automatic equipment BELSORP MINI, BEL JAPAN, after the material was outgassed at 150 °C for 6 hours. The specific surface areas (SBET) were calculated using the Brunauer–Emmett–Teller (BET) method, applying the Rouquerol consistency criteria to ensure the appropriate selection of the linear range.[25] Dynamic vapor sorption (DVS) was used to study the water adsorption characteristics of ZIF-71(ClBr)-SE and to determine the material's hydrophobic nature. The sample of ZIF-71(ClBr)-SE was activated by heating to 200 °C at 10^{-6} Torr for 2 hours. The method was programmed to perform full water sorption and desorption cycles.

Static batch adsorption

Batch adsorption experiments were carried out to measure the single- and ternary-component adsorption capacity of butanol, acetone, and ethanol in dilute aqueous solutions onto ZIF-71, ZIF-71(ClBr)-SE, and ZIF-8 at 25 °C. Typically, 100 mg of adsorbent were added in a 10 mL capacity close bottle containing 5 mL of the solution and stirred at 150 rpm. After 24 h, the liquid phase was analysed using a gas chromatograph (SHIMADZU, GC-2030) with a flame ionization detector (FID). The GC column was SH-Stabilwax-DA (60 m × 0.25 mm × 0.25 mm film thickness). The mobile carrier gas phase through the column was helium at 2 mL min^{-1}, and the temperature of the column was 190 °C. All static batch adsorptions were repeated thrice. The adsorbed quantity q, expressed as grams of solute per gram of adsorbent material (mg g^{-1}), was calculated using eqn (1):

$$q = \frac{V}{m}(C_0 - C_t) \tag{1}$$

where C_0 is the initial concentration, and C_t is the concentration at time t. V is the volume of the solution, and m is the mass of the adsorbent.

Adsorption selectivity (S_{ik}) of component i, corresponding to butanol in the ternary-component solution, was determined as a function of the adsorption capacity (q) of the adsorbent and the initial concentration (C_0) of the solute in the solution using eqn (2):

$$S_{ik} = \frac{q_i \sum_{k=2}^{3} C_{k,0}}{C_{i,0} \sum_{k=2}^{3} q_k} \tag{2}$$

Density functional theory calculation model and method

Density functional theory (DFT) calculations were performed to elucidate the adsorption mechanism in ZIF-71(ClBr)-SE at microscopic level. Each structure was analysed using plane-wave DFT calculations as implemented in the Spanish Initiative for Electronic Simulations with Thousands of Atoms package (SIESTA) package. The accuracy of molecular interactions descriptions depends on the appropriate selection of the functional and basis set. The generalized gradient approximation (GGA) is a scheme that use both the density and its gradient at each point, generally providing more accurate results compared to the local density approximation (LDA). Calculations were performed using Perdew–Burke–Ernzerhof (PBE) functional, an GGA functional for electron exchange and correlation. The Trollier–Martin pseudopotentials descriptions was used for all core and semicore of species, while valence electrons were described with double zeta basis plus polarization functions (DZP). At the Γ-point geometry optimizations were performed employing the conjugate gradient algorithm until the forces on each atom were less than 0.04 eV Å^{-1}. The projector augmented wave (PAW) technique was used with a cutoff of 350 eV to improve energy precision and efficiency. Atomic partial charges were obtained by the Hirshfeld method which derives charge values from an analysis of the electrostatic potential surface.

Binding energies of each adsorbate on ZIF-71 or ZIF-71 (ClBr)-SE were estimated as their interaction energy through the eqn (3):

$$E = E_{AB} - (E_A + E_B) \tag{3}$$

where E_A is the energy of a single optimized adsorbate, E_B is the energy of a single optimized ZIF cluster, and E_{AB} corresponds to the energy of the optimized ZIF-adsorbate system.[26]

Results and discussion

Characterization

The phase and crystallinity of the ZIF-71(ClBr)-SE were verified by PXRD (Fig. S1†).[23] The well-defined reflections in the XRD pattern indicate to the formation of a well-ordered framework. The PXRD pattern was compared with the simulated pattern of ZIF-71, showing a well-matched with the main peaks at 2θ (≈4.4°, 6.2°, and 7.5°). This shows that ZIF-71(ClBr)-SE is isostructural with ZIF-71 and exhibits an RHO topology.[27]

The thermal stability of activated ZIF-71(ClBr)-SE was investigated using TGA, as shown in Fig. 1. The sample showed no weight loss between 25 and 270 °C, indicating the absence of physically adsorbed water and crystal water (hydrates), which typically release around 110 °C and 170 °C, respectively. A sudden weight loss of 28% occurred between 390 and 420 °C, with the change centred at 405 °C. A second significant thermal event, centred at 500 °C, accounted for a 52% weight loss. The final thermal event, centred at 626 °C, represented a 15% weight loss. The remaining 4.7% weight above 700 °C corresponds to ZnO ash, indicating the zinc content in the sample. This thermal behaviour aligns with the literature reported by Li *et al.* for ZIF-71.[28] The initial weight loss can be attributed to the onset of the ZIF-71(ClBr)-SE framework decomposition. The second weight loss corresponds to the decomposition of organic components and the release of Cl and Br. The third stage of weight loss is associated with the further removal of organic linkers from the main ZIF-71 structure, as reported by Japip *et al.*[29]

Fig. 2 shows HAADF-STEM images and particle size measurements for the synthesized ZIF-71(ClBr)-SE. The ZIF-71 (ClBr)-SE particles exhibit a polygonal morphology (Fig. 2a and b) and have a particle size range of 37.5 to 337.5 nm, with the largest population around 137.5 nm (Fig. 2c). These particles are smaller than those reported for other ZIF-71 MOFs,[30,31] which could enhance their adsorption capacities.

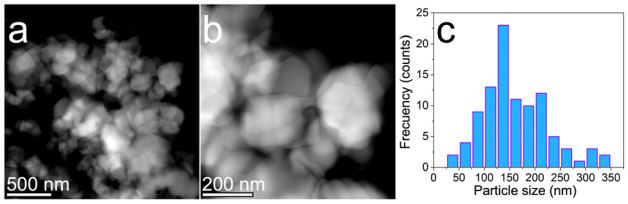

Fig. 2 Morphological characterization of ZIF-71(ClBr)-SE: (a) HAADF-STEM images taken at 28.5 kX; (b) HAADF-STEM recorded at 80 kX; (c) bar chart showing the particle size distribution.

Nitrogen physisorption experiment were performed on ZIF-71(ClBr)-SE and ZIF-71 to assess their textural properties (Fig. 3). The materials displayed type I isotherms, which are characteristic of microporous solids according to the IUPAC classification. The BET areas (S_{BET}) of ZIF-71(ClBr)-SE and ZIF-71 were determined to be 952 and 814 $m^2\ g^{-1}$, respectively. From the isotherm data and using the non-linear DFT method, the pore size distribution for ZIF-71(ClBr)-SE was calculated (Fig. S2†), yielding a value of 15.4 Å similar to the value reported in the literature for ZIF-71.[32] No hysteresis was observed in the isotherm for ZIF-71(ClBr)-SE, which also confirms the absence of interplanar voids, as shown in the TEM analysis image (Fig. 2).

The water adsorption isotherm of ZIF-71(ClBr)-SE demonstrated a minimal water uptake, even at increasing humidity levels[16] exhibiting a maximum uptake of 0.54% at 95%RH and 25 °C (Fig. 4). The water uptake in ZIF-71(ClBr)-SE was initially very low but significantly increased beyond P/P_0 = 0.4. This can be attributed to a weak interaction between the ZIF-71(ClBr)-SE pore surface and isolated water molecules. Nevertheless, after more water molecules are adsorbed, the adsorbate–adsorbate interactions encourage the adsorption of further water molecules, resulting in a convex curvature in the high relative

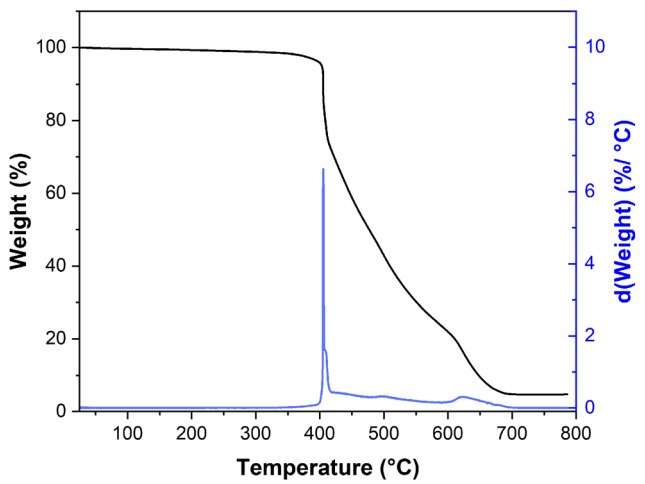

Fig. 1 Thermogravimetric analysis curve and its derivative of ZIF-71 (ClBr)-SE.

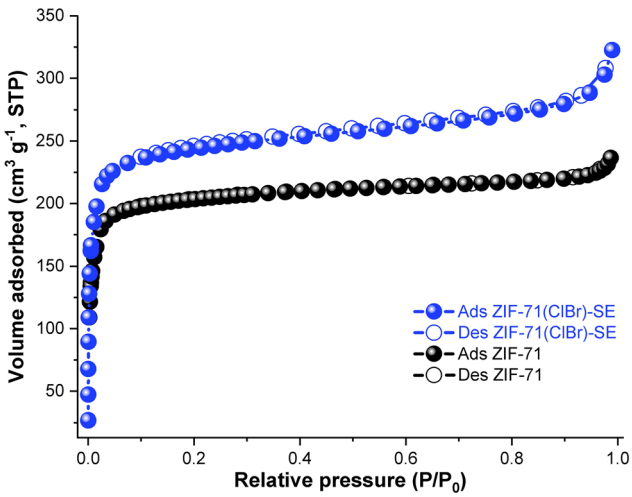

Fig. 3 Nitrogen adsorption/desorption isotherms for ZIF-71 and ZIF-71 (ClBr)-SE.

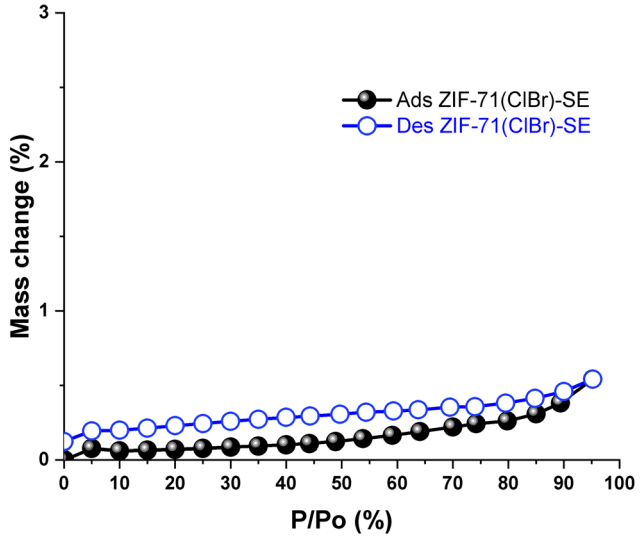

Fig. 4 Water sorption isotherm for sample ZIF-71(ClBr) SE at 25 °C.

pressure region. Therefore, the strong hydrophobicity of the pores is a key factor influencing water uptake.

A rather different adsorption shape was exhibited for ZIF-71 and ZIF-8 (the less hydrophobic of these ZIFs). In the case of ZIF-71, a nearly linear uptake can be assumed. At $P/P_0 < 0.9$, the water uptake was higher than ZIF-71(ClBr)-SE indicating that the Br atom in the imidazole ligand enhances the hydrophobic nature of ZIF-71. Although at first glance one might assume that water was adsorbed more favourably on ZIF-71 (ClBr)-SE than ZIF-71 at $P/P_0 > 0.9$, this could not be the case. Given that adsorption capacity decreases with increasing temperature, it is reasonable to expect that the water uptake of ZIF-71 at 25 °C would be higher than at 35 °C. In this way, the surface of ZIF-71(ClBr)-SE can be more hydrophobic. To further support this statement, comparing water adsorption isotherms could be useful (Fig. 5).[24]

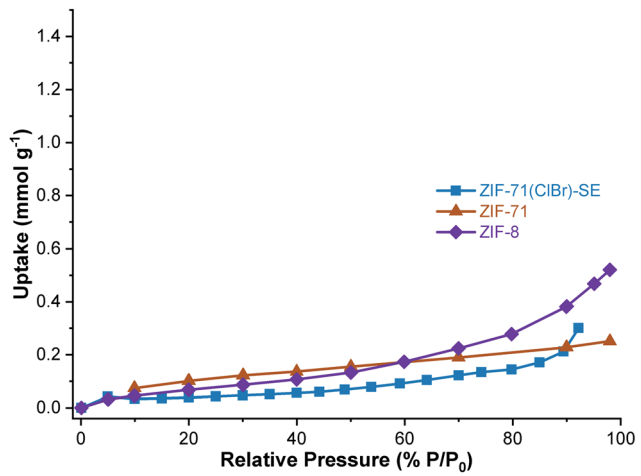

Fig. 5 Water adsorption isotherms in ZIF-8, ZIF-71 (at 308 K)[24] and ZIF-71(ClBr)-SE (at 298 K).

The hydrophobicity of the external surface of MOFs is frequently assessed by measuring its water contact angle. The water contact angles of ZIF-8, ZIF-71, and ZIF-71(ClBr)-SE have been previously reported, with ZIF-71(ClBr)-SE showing the highest value at 130°, compared to 108° for ZIF-8 and 126.79° for ZIF-71.[23] This higher contact angle for ZIF-71(ClBr)-SE highlights and confirms its enhanced hydrophobic nature.

Adsorption capacity in single- and ternary-component system

Adsorption equilibrium experiments were carried out on a single-component ABE system using three hydrophobic ZIFs: ZIF-8 (Basolite Z1200), ZIF-71 and, ZIF-71(ClBr)-SE (Fig. 6) at room temperature in dilute aqueous solution (4.0 wt%). As shown in Fig. 7, the ethanol adsorption capacities of ZIF-8, ZIF-71(ClBr)-SE, and ZIF-71 were lower compared to those of acetone and butanol. This behaviour may be attributed to the hydrophobic nature of the ZIFs and the polarity of ethanol.[33–35] For ZIF-8, factors such as the lower polarizability of ethanol, the kinetic diameter of ethanol (4.5 Å), and the pore aperture (3.4 Å) may further influence the reduced adsorption of ethanol.[36,37] In the case of ZIF-71, it features a larger pore aperture (5.1 Å) than the kinetic diameter of ethanol, suggesting that the reduced ethanol adsorption may be rationalized in terms of the relative hydrophobicity of ZIF-71 and the polarity of ethanol. Although the pore size could allow ethanol molecules to access the internal structure of ZIF-71, the hydrophobic framework likely limits interactions with the polar ethanol, thereby reducing adsorption efficiency.[38] Among the ZIFs tested, ZIF-8 exhibited the highest adsorption capacity for all components, likely due to its larger specific surface area (~1350 $m^2\ g^{-1}$) in comparison to ZIF-71 (814 $m^2 g^{-1}$) and ZIF-71(ClBr)-SE (952 $m^2\ g^{-1}$).

ZIF-71 and ZIF-8 showed higher adsorption capacities for butanol compared to acetone and ethanol, which aligns with the literature reports.[36,37,39,40] However, an unexpected result was observed in the case of ZIF-71(ClBr)-SE. Despite its greater hydro-

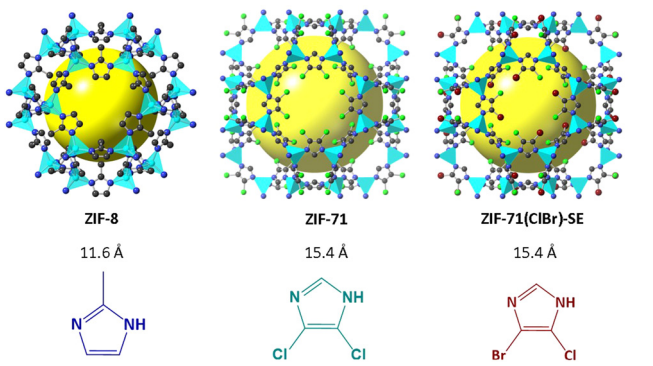

Fig. 6 Structural representation of ZIF-8 and ZIF-71 along the [100] direction, and schematic representation of the ZIF-71(ClBr)-SE crystal structure based on ZIF-71. Pore diameter and imidazole ligand derivatives are shown. All hydrogen atoms have been omitted for clarity. (Atom colours: H, white; C, black; N, blue; Cl, green; Br, red; Zn, cyan polyhedral; yellow spheres indicate free space within the framework). (Colour online).

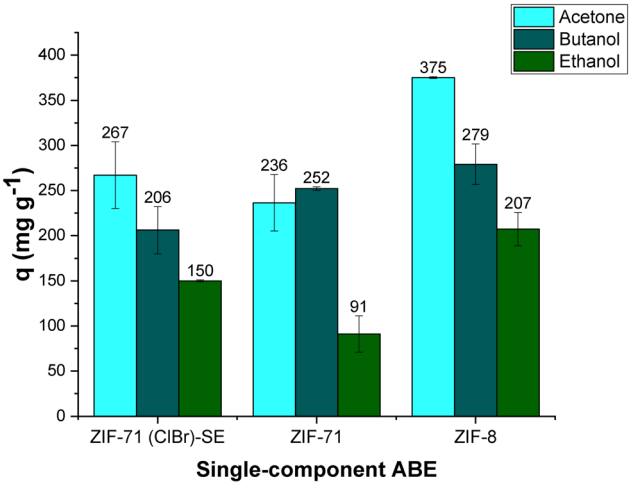

Fig. 7 Adsorption capacities of single-component of acetone, butanol and ethanol of ZIF-8, ZIF-71, and ZIF-71(ClBr)-SE, conditions: adsorbent dose 20 g L^{-1}, initial concentration of 4.0 wt%, and 25 °C.

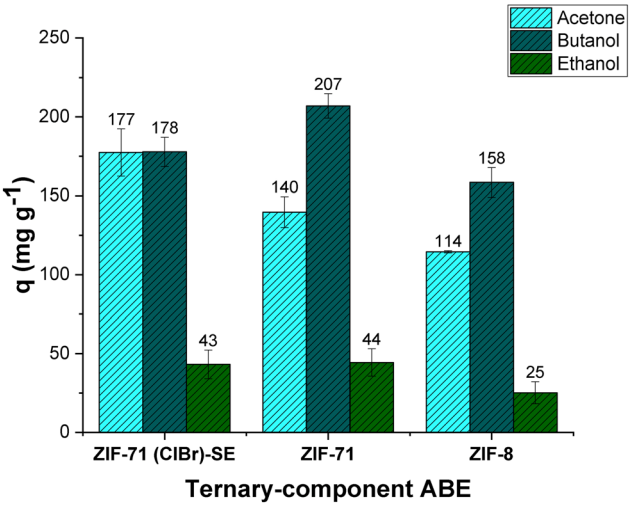

Fig. 8 Adsorption capacities of ternary-component of acetone, butanol, and ethanol of ZIF-8, ZIF-71, and ZIF-71(ClBr)-SE, conditions: adsorbent dose 20 g L^{-1}, initial concentration of 4.0 wt%, and 25 °C.

phobicity compared to ZIF-8 and ZIF-71,[23] ZIF-71(ClBr)-SE showed a higher adsorption capacity for acetone than for butanol and ethanol. While hydrophobicity plays a significant role in adsorption, the available surface area and pore accessibility are also critical in determining adsorption capacity. ZIF-71(ClBr)-SE has a lower surface area compared to ZIF-8, which could limit the number of adsorption sites available for larger molecules like butanol (kinetic diameter 5 Å). Acetone, being a smaller molecule with a kinetic diameter 4.7 Å and less steric hindrance, may access these pores more easily, resulting in higher adsorption despite the material's hydrophobic nature.[36,41]

Adsorption equilibrium experiments were conducted on ternary-component ABE system to assess competitive adsorption and selectivity. The adsorption capacities of the three hydrophobic materials investigated are shown in Fig. 8. The adsorption capacities for acetone, butanol, and ethanol in the ternary-component system were noticeably lower compared to single-component systems, suggesting the occurrence of competitive adsorption among the three components.[37] As expected, ethanol exhibited the lowest adsorption across all tested materials (<44 mg g^{-1}), consistent with the results from single-component tests. This result also suggests that these hydrophobic ZIFs do not exhibit selectivity towards ethanol under the tested conditions.[37,42]

The competitive adsorption on ZIF-71 and ZIF-8 demonstrated an affinity order of butanol > acetone > ethanol, consistent with the single-component adsorption findings. This suggests that the affinity for the solute decreases as the polarity increases.[42] Among the three ZIFs tested, ZIF-71 exhibited the highest butanol adsorption capacity in the ternary-component system and greater butanol selectivity over acetone (1.43) compared to ZIF-8. Even though ZIF-71 has a lower surface area compared to ZIF-8, its higher affinity and adsorption capability for butanol may be explained due to its hydrophobic character.[24,41]

In contrast, ZIF-8 showed the lowest adsorption capacity for butanol but the highest selectivity for butanol over acetone and ethanol, as depicted in Fig. 8 and 9. According to the literature, ZIF-8 has a SOD structure with a pore opening size of 3.4 Å, which is smaller than the kinetic diameter of butanol (5 Å).[37,43,44] However, studies have demonstrated that ZIF-8 exhibits a flexible structure, allowing it to effectively adsorb butanol despite its pore size.[36] This flexibility of ZIF-8 arises from the rotation of the N–Zn–N bond, a feature absent in the structure of ZIF-71 due to the presence of halogenated atoms in the imidazole ligand.[45]

Regarding ZIF-71(ClBr)-SE, this material exhibited similar adsorption capacities for both acetone and butanol (177 mg g^{-1}), suggesting no competitive adsorption between the two solvents. The substitution of a chlorine (Cl) atom with a bromine (Br) atom in the imidazole organic ligand was intended to enhance the hydrophobic character of ZIF-71 (ClBr)-SE, which was expected to increase its affinity for

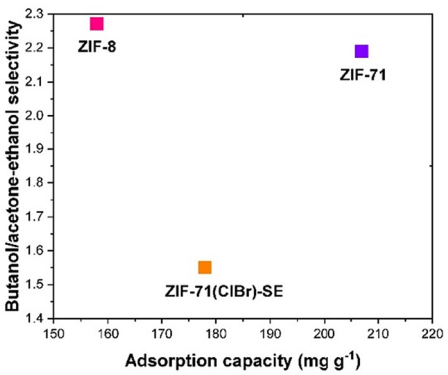

Fig. 9 Adsorption selectivity for butanol/acetone–ethanol as a function of the butanol uptake for ZIF-71(ClBr)-SE, ZIF-71, and ZIF-8.

butanol. However, similar to the single-component system, the ZIF-71(ClBr)-SE could not achieve a higher adsorption capacity of butanol as a result of its increased hydrophobicity in the ternary-component system.

These findings may be attributed to two key factors. First, since ZIF-71(ClBr)-SE is isostructural with ZIF-71, as indicated by the XRD pattern and pore distribution, the pore aperture is likely comparable. However, it is possible that inclusion of bromine atom resulted in a reduction in pore opening (<5.1 Å) due to the steric hindrance of the bromine atom in a less flexible structure. Second, the lower specific surface area of ZIF-71 (ClBr)-SE compared to ZIF-71 and ZIF-8 could be a significant factor contributing to its adsorption behaviour.

Microscopic details from calculated properties

Optimized geometrical parameters for the ZIFs (ZIF-71 and ZIF-71(ClBr)-SE) are shown in Table S1.† The obtained structure is in good agreement with the experimental data results.[27] Interactions energies and interatomic distances relevant for the description of the interaction between butanol or ethanol with ZIF are displayed in Table S2.† Reference labels for certain atoms in the ZIF structures are presented in (Fig. 10). In the case of ZIF-71(ClBr)-SE, the C2 atom is bonded to brime, while in ZIF-71, the C2 atom is bonded to chlorine. Adsorption doees not significantly alter most of the intramolecular parameters of the studied ZIFs, with changed being less than 1%. This minimal variation ensures that the imidazole ligand retains its characteristics for non-covalent interactions.[46] A representative set is depicted in Table S3.†

Alcohol molecules display two forms of approaching toward interactions sites of ZIF, mainly through their methyl group or their hydroxy group, the last motif is 2.5 to 3.5 times more stable than the first motif. Nonetheless, the reduction in dihedral angle among the atoms C1–N1–N3–C4 (Fig. S3†), an intramolecular parameter of ZIF, is 39%, three times larger than the reduction provoked when alcohols interact through

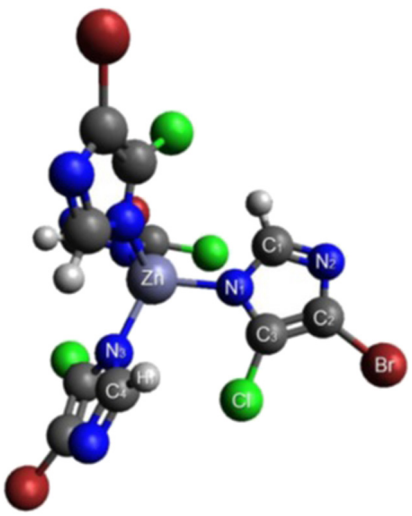

Fig. 10 Reference atomic labels for ZIF-71(ClBr)-SE and ZIF-71.

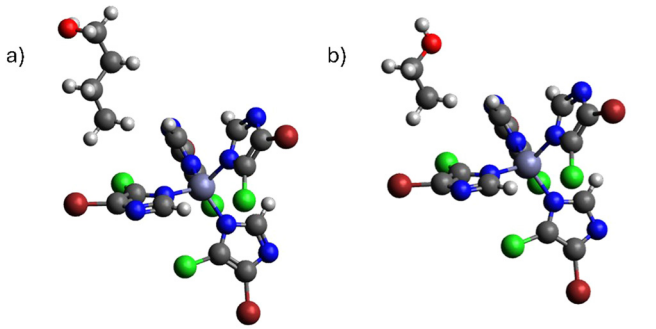

Fig. 11 Illustration of the DFT simulated interaction in (a) ZIF-71(ClBr)-SE/butanol and (b) ZIF-71(ClBr)-SE/ethanol system through methyl. Color code: Zn, lilac; O, red; Br, metallic red; N, blue; Cl, green; C, grey; H, white.

methyl. Therefore, this preferred orientation is more likely to occur experimentally because it generates less deformation and stress within the MOF structure (Fig. 11).

In principle, acetone presents multiple modes of interaction ZIF sites due to its ability to engage through various orientations *via* its carbonyl and methyl groups.[47] If the molecular plane of acetone is more aligned to the imidazole plane, acetone can point its carbonyl oxygen in order to establish pseudo hydrogen bonds with –CH of adjacent imidazole ligand while interacting with carbon C3 and simultaneously approaching its methyl groups to the halogen on it. However, when carbonyl carbon interacts closely with C2 it causes deviation from semi-symmetric to non-symmetric distances from methyl carbons toward the halogen on it. For such cases the values of the geometrical parameters displayed in Table S5,† indicates that the asymmetry in distances is around 10% larger than in the more symmetric patterns (Fig. 12).

As in the case of alcohols, structures with enhanced interaction energies in general present larger deviation of the intramolecular dihedral angle of ZIF, hence they are less likely to occur experimentally. These highlights the role of the sym-

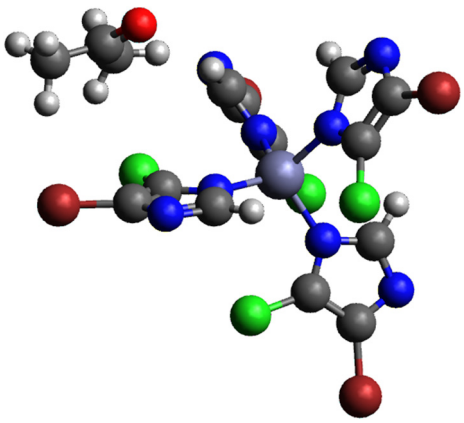

Fig. 12 Illustration of the DFT simulated interaction in ZIF-71(ClBr)-SE/acetone system aligned to the imidazole plane. Color code: Zn, lilac; O, red; Br, metallic red; N, blue; Cl, green; C, grey; H, white.

metric interactions patterns which prevents MOF structure deformation. Exceptions to this observation are some non-symmetric structures with a reduced dihedral deformation, they occur when the molecular plane of acetone tends to be less aligned to the imidazole plane. Steep vertical orientation require that acetone directs only one of its methyl groups towards ZIF.

The computational results, when compared with experimental findings for single-component adsorbent systems, reveal a contrast with the observed preference for butanol on ZIF-71 over ZIF-71(ClBr)-SE. This reveals that complex phenomena in solution compete more for the polar head of butanol than for ethanol, when it is being absorbed. This may be due to its larger alkyl tail, suggesting a cooperative mechanism of adsorption. It also indicates that hydrophobic solvation is accentuated near ZIF-71(ClBr)-SE surface. In the other hand, the charge transferred from the ZIF to butanol, −0.048e, is about 6.5 times larger when is methyl oriented than hydroxy oriented. The excess of charge could also explain its experimental adsorption preference on ZIF-71, in which hydrophobic solvation is less marked (Table S4 and Fig. S4†).

The compromised between a larger variety of patterns that acetone can interact with ZIF in one hand, and its larger dipole moment in the other, could explain the similar acetone uptake in solution observed for ZIF when considering the experimental error bars. Additionally, the charge transferred from ZIF to acetone for some of the symmetric and non-symmetric orientation patterns with less dihedral distortion, is about 73% to 94% of the charge transferred to butanol (Table S4 and Fig. S4†), such small to medium difference may cause the apparent larger preference of adsorption on ZIF-71 (ClBr)-SE which attains an increased hydrophobic solvation near its surface.[48]

Conclusions

In summary, the performance of hydrophobic ZIF-71(ClBr)-SE was studied regarding its adsorption capacity for butanol *versus* acetone and ethanol in an ABE ternary-component system. These results were compared to its analogous ZIF-71 and representative hydrophobic ZIF (ZIF-8). Our results showed that in the single- and ternary component system adsorption experiments, ZIF-71 and ZIF-8 showed that adsorption capacities follow the order butanol > acetone > ethanol. However, the ZIF-71(ClBr)-SE with an increased hydrophobic character, exhibited a higher adsorption capacity for acetone than butanol in a singular-component system. While the incorporation of the bromine atom into the zeolite ligand enhanced the hydrophobic nature of ZIF-71(ClBr)-SE, it seems that the bromine atom hampered the pore aperture, reducing the likelihood of butanol diffusion. Additionally, DFT calculations offered insights into the interactions within the solute-ZIF system. Specifically, alcohol molecules tend to interact with the ZIF through their methyl groups, as this causes less structural deformation. For acetone, its ability to interact with ZIF through various patterns, along with the charge transfer from ZIF to acetone in specific orientations with minimal dihedral distortion compared to alcohols, may contribute to the observed preference for adsorption on ZIF-71(ClBr)-SE.

Author contributions

Norma Tiempos-Flores: conceptualization, investigation, writing – original draft, formal analysis. Sandra Pioquinto-García: writing – review & editing, formal analysis. Eugenio Hernández-Fernández: writing – review & editing, visualization. Victor M. Ovando-Medina: methodology, formal analysis, writing – review & editing. Oscar I. Arillo-Flores: formal analysis, methodology, software, data curation. Marco A. Garza-Navarro: methodology, formal analysis, validation. Nancy E. Davila-Guzman: supervision, funding acquisition, project administration, resources, writing – review & editing.

Data availability

The data supporting this article have been included as part of the ESI.†

Conflicts of interest

There are no conflicts to declare.

Acknowledgements

The authors thank the Southeast Mexico National Supercomputer Laboratory, belonging to the CONAHCYT network of national laboratories, for the computational resources, support, and technical assistance provided in Project 202003049n, 20230360n and 202303067n.

References

1 Balance Nacional de Energía | Secretaría de Energía | Gobierno | gob.mx, **https://www.gob.mx/sener/articulos/balance-nacional-de-energia-296106**, (accessed 31 August 2024).
2 Executive summary – World Energy Outlook 2023 – Analysis - IEA, **https://www.iea.org/reports/world-energy-outlook-2023/executive-summary**, (accessed 31 August 2024).
3 Key Findings | United Nations, **https://www.un.org/en/climatechange/science/key-findings**, (accessed 31 August 2024).
4 M. N. A. M. Yusoff, N. W. M. Zulkifli, B. M. Masum and H. H. Masjuki, *RSC Adv.*, 2015, **5**, 100184–100211.
5 K. R. Szulczyk, *Int. J. Energy Environ.*, 2010, **1**, 501–512.

6 A. Pugazhendhi, T. Mathimani, S. Varjani, E. R. Rene, G. Kumar, S. H. Kim, V. K. Ponnusamy and J. J. Yoon, *Fuel*, 2019, **253**, 637–646.
7 D. S. Nabila, R. Chan, R. R. P. Syamsuri, P. Nurlilasari, W. A. A. Q. I. Wan-Mohtar, A. B. Ozturk, N. Rossiana and F. Doni, *Curr. Res. Microb. Sci.*, 2024, **7**, 100250.
8 D. Cai, J. Wen, Y. Zhuang, T. Huang, Z. Si, P. Qin and H. Chen, *Sep. Purif. Technol.*, 2022, **298**, 121244.
9 N. Qureshi, S. Hughes, I. S. Maddox and M. A. Cotta, *Bioprocess Biosyst. Eng.*, 2005, **27**, 215–222.
10 N. Abdehagh, F. H. Tezel and J. Thibault, *Biomass Bioenergy*, 2014, **60**, 222–246.
11 J. L. C. Rowsell and O. M. Yaghi, *Microporous Mesoporous Mater.*, 2004, **73**, 3–14.
12 R. Banerjee, A. Phan, B. Wang, C. Knobler, H. Furukawa, M. O'Keeeffe and O. Yaghi, *Science*, 2008, **319**, 939–943.
13 J. Cousin Saint Remi, T. Rémy, V. Van Hunskerken, S. van de Perre, T. Duerinck, M. Maes, D. De Vos, E. Gobechiya, C. E. A. Kirschhock, G. V. Baron and J. F. M. Denayer, *ChemSusChem*, 2011, **4**, 1074–1077.
14 K. Jayaramulu, F. Geyer, A. Schneemann, Š. Kment, M. Otyepka, R. Zboril, D. Vollmer, R. A. Fischer, K. Jayaramulu, A. Schneemann, R. A. Fischer, Š. Kment, M. Otyepka, R. Zboril, F. Geyer and D. Vollmer, *Adv. Mater.*, 2019, **31**, 1900820.
15 L. Gan, A. Chidambaram, P. G. Fonquernie, M. E. Light, D. Choquesillo-Lazarte, H. Huang, E. Solano, J. Fraile, C. Viñas, F. Teixidor, J. A. R. Navarro, K. C. Stylianou and J. G. Planas, *J. Am. Chem. Soc.*, 2020, **142**, 8299–8311.
16 J. Wang, J. Wu, B. Zheng, J. Wang, Q. Shi and J. Dong, *Chem. Eng. Sci.*, 2021, **248**, 117251.
17 J. Song, Q. Meng, J. Wang, X. Guo, P. Wei, J. Dong and Q. Shi, *Sep. Purif. Technol.*, 2023, **312**, 123371.
18 D. Princík, V. Zeleňák, J. Bednarčík, J. Elečko, J. Macko, T. Zelenka, R. Gyepes and E. Dutková, *Polyhedron*, 2024, **247**, 116739.
19 S. Liu, P. Li, Y. Zhang, X. Gao, G. Wang, S. Song and X. Zhao, *Environ. Funct. Mater.*, 2024, DOI: **10.1016/j.efmat.2024.07.004**.
20 X. Quan, J. Zhang, L. Yin and Y. Tian, *Colloids Surf., A*, 2024, **695**, 134156.
21 Y. Zhou, Z. Li, X. Xu, X. Li, Y. Qing, Q. Huang and Y. Wu, *Sep. Purif. Technol.*, 2024, **346**, 127478.
22 A. Priimagi, G. Cavallo, P. Metrangolo and G. Resnati, *Acc. Chem. Res.*, 2013, **46**, 2686–2695.
23 N. Tiempos-Flores, E. Hernández-Fernández, A. Rico-Barragan, J. Raziel Álvarez, I. Juárez-Ramírez, M. A. Garza-Navarro, J. Rodríguez-Hernández, A. Fonseca-García, D. J. Michaelis and N. E. Davila-Guzman, *Polyhedron*, 2022, **217**, 115736.
24 K. Zhang, R. P. Lively, W. J. Dose and R. R. Chance, *Chem. Commun.*, 2013, **49**, 3245–3247.
25 J. Rouquerol, P. Llewellyn and F. Rouquerol, *Stud. Surf. Sci. Catal.*, 2007, **160**, 49–56.
26 Z. Qiao, Z. Wang, C. Zhang, S. Yuan, Y. Zhu and J. Wang, *AIChE J.*, 2012, **59**, 215–228.
27 R. Banerjee, H. Phan, M. O'Keeffe and O. M. Yaghi, *Science*, 2008, **319**, 939–943.
28 Y. Li, L. H. Wee, J. A. Martens and I. F. J. Vankelecom, *J. Mater. Chem. A*, 2014, **2**, 10034–10040.
29 S. Japip, H. Wang, Y. Xiao and T. S. Chung, *J. Membr. Sci.*, 2014, **467**, 162–174.
30 H. Yin, M. D. Cay-Durgun and M. L. Lind, *Polymer*, 2020, **195**, 1–26.
31 X. Liu, J. Wang, L. Fang, Y. Ban and M. He, *Process Saf. Environ. Prot.*, 2024, **189**, 664–673.
32 J. Wang, J. Wu, B. Zheng, J. Wang, Q. Shi and J. Dong, *Chem. Eng. Sci.*, 2022, **248**, 117251.
33 R. Goerlitz, L. Weisleder, S. Wuttig, S. Trippel, K. Karstens, P. Goetz and H. Niebelschuetz, *Adsorption*, 2018, **24**, 95–104.
34 J. Wu, W. Zhuang, H. Ying, P. Jiao, R. Li, Q. Wen, L. Wang, J. Zhou and P. Yang, *Biotechnol. Prog.*, 2015, **31**, 124–134.
35 J. Cousin Saint Remi, G. Baron and J. Denayer, *Adsorption*, 2012, **18**, 367–373.
36 C. Gao, Q. Shi and J. Dong, *CrystEngComm*, 2016, **18**, 3842–3849.
37 C. Gao, J. Wu, Q. Shi, H. Ying and J. Dong, *Microporous Mesoporous Mater.*, 2017, **243**, 119–129.
38 J. Wang, J. Wu, B. Zheng, J. Wang, Q. Shi and J. Dong, *Chem. Eng. Sci.*, 2022, **248**, 117251.
39 F. Raganati, A. Procentese, G. Olivieri, M. E. Russo, P. Salatino and A. Marzocchella, *Sep. Purif. Technol.*, 2018, **191**, 328–339.
40 J. C. Saint Remi, G. Baron and J. Denayer, *Adsorption*, 2012, **18**, 367–373.
41 X. Dong and Y. S. Lin, *Chem. Commun.*, 2013, **49**, 1196–1198.
42 A. Oudshoorn, L. A. M. van der Wielen and A. J. J. Straathof, *Biochem. Eng. J.*, 2009, **48**, 99–103.
43 X. C. Huang, Y. Y. Lin, J. P. Zhang and X. M. Chen, *Angew. Chem., Int. Ed.*, 2006, **45**, 1557–1559.
44 R. Banerjee, A. Phan, B. Wang, C. Knobler, H. Furukawa, M. O'Keeffe and O. M. Yaghi, *Science*, 2008, **319**, 939–943.
45 A. F. Möslein and J. C. Tan, *J. Phys. Chem. Lett.*, 2022, **13**, 2838–2844.
46 H. H. Huang, Y. S. Wang and S. D. Chao, *ACS Omega*, 2022, **7**, 20059–20080.
47 D. A. Shitov, D. V. Krutin and E. Y. Tupikina, *J. Comput. Chem.*, 2024, **45**, 1046–1060.
48 D. Mester and M. Kállay, *J. Chem. Theory Comput.*, 2022, **18**, 1646–1662.